Two-Dimensional Transonic Aerodynamic Design Method

Michael B. Giles* and Mark Drela†
Massachusetts Institute of Technology, Cambridge, Massachusetts

This paper demonstrates the capabilities of a new transonic, two-dimensional design method, based on the simultaneous solution of multiple streamtubes, coupled through the position of, and pressure at, the streamline interfaces. This allows the specification of either the airfoil shape (direct, analysis mode) or the airfoil surface pressure distribution (inverse, design mode). The nonlinear system of equations is formulated in a conservative manner, which guarantees the correct treatment of shocks, and is solved by a rapid Newton solution method. Viscous effects can also be included through a coupled integral boundary-layer analysis. The first set of results shows the effect of different far-field treatments, demonstrating the improvement in accuracy obtained by including the second-order doublet terms in addition to the usual first-order vortex term. The results are also compared to those obtained by specifying straight far-field streamlines (corresponding to solid-wall wind-tunnel experiments) or constant far-field pressure (corresponding to freejet experiments) to show the sensitivity to the far-field distance. In the second set of results, the design method is used to design a transonic airfoil with $C_l = 1.000$ at $M_\infty = 0.70$. It is shown that the off-design performance is improved by specifying a surface pressure distribution with a very weak shock.

Nomenclature

C_d	= drag coefficient
C_l	= lift coefficient
D_x, D_y	= far-field doublet strengths
h_0	= stagnation enthalpy
m	= mass flux
M_∞	= freestream Mach number
p	= pressure (in streamtubes)
q	= speed
$\mathbf{q}$	= velocity
Re	= Reynolds number
$\mathbf{s} \equiv \mathbf{q}/q$	= unit vector in flow direction
x,y	= coordinates
γ	= ratio of specific heats
Γ	= far-field vortex strength
Π	= pressure (on streamlines)
ρ	= density
Σ	= far-field source strength
Φ	= far-field potential

I. Introduction

MOST computational methods for predicting transonic flow over airfoils are analysis methods, which predict the surface pressure distribution on an airfoil with a specified geometry. Relatively few methods address the aerodynamic designer's task of designing more efficient airfoils. Those that do, fall into two categories.

The first category is optimization methods, which couple a conventional analysis method with an optimization algorithm to modify iteratively the geometry in order to minimize some "cost" function, such as the drag or the difference between the actual and desired surface pressure distributions. The methods of Vanderplaats[1] and Hicks[2] are examples of this category. The principal disadvantage of this approach is that it is very time-consuming computationally, making it both expensive and inconvenient for use as an everyday design procedure.

The second category is inverse design methods, in which one specifies the surface pressure distribution and the method calculates the corresponding airfoil geometry. This approach was pioneered by Lighthill[3] for incompressible flow using a conformal mapping technique. For transonic flows, the two principal approaches are potential methods and hodograph methods. The potential methods, such as the GRUMFOIL code of Volpe and Melnik,[4] solve the nonlinear, isentropic, full-potential equations in the physical plane. The hodograph methods, of which the method by Bauer et al.[5] was the first and remains the most widely used, solve the full-potential equations in the hodograph plane in which the equations are linear. Both methods have been extended to include viscous effects through a boundary-layer displacement thickness calculated using an integral boundary-layer analysis. The potential methods are more flexible because they also have the capability to be used in a direct, analysis mode so that, after designing a new airfoil, the same method can then analyze its off-design performance. A limitation of both approaches is the assumption of isentropic flow, which leads to an incorrect treatment of shocks. The advantage of these methods over the optimization methods previously described is that they are much faster, allowing interactive design at workstations.

This paper presents results obtained using a new analysis/design code, ISES, which has been developed over the last three years.[6-9] In concept, it has similarities to both the streamline curvature analysis methods used in turbomachinery calculations and the full potential inverse design methods. Its origins lie in research on solving the Euler equations for quasi-one-dimensional streamtubes.[10,11] The current method is the natural two-dimensional extension of this work, which treats the two-dimensional flow as a set of streamtubes coupled through the position of, and pressure at, the streamline interfaces. The unknown variables are both the velocity of the fluid and the position of the streamlines. The discrete Euler equations are assembled as a system of nonlinear equations and solved simultaneously using the Newton method. Unlike the full-potential methods, this method solves the Euler equations in conservative integral form and so correctly handles shocks. As with the potential methods at the airfoil surface, one can either specify the position of the surface streamline (direct, analysis

Received July 7, 1986; revision received Dec. 9, 1986.

*Charles Stark Draper Assistant Professor, Department of Aeronautics and Astronautics. Member AIAA.

†Assistant Professor, Department of Aeronautics and Astronautics. Member AIAA.

mode) or the pressure on the surface (inverse, design mode). Viscous effects can also be included through a coupled integral boundary-layer analysis, which is the subject of a companion paper.[12]

II. Discrete Euler Equations

The steady-state finite-volume equations are derived from the integral form of the mass, momentum, and energy conservation laws.

$$\oint_{\partial V} \rho(\boldsymbol{q}\cdot\boldsymbol{n})\,\mathrm{d}l = 0 \tag{1}$$

$$\oint_{\partial V} [\rho(\boldsymbol{q}\cdot\boldsymbol{n})\boldsymbol{q} + p\boldsymbol{n}]\,\mathrm{d}l = 0 \tag{2}$$

$$\oint_{\partial V} \rho(\boldsymbol{q}\cdot\boldsymbol{n})h_0\,\mathrm{d}l = 0 \tag{3}$$

where the integration is around a closed curve ∂V with normal $\boldsymbol{n}$.

The discrete equations are obtained by applying these equations on an intrinsic finite-volume grid in which one family of grid lines corresponds to streamlines. A typical conservation cell is shown in Figs. 1 and 2. Its four nodes are at the midpoints of the streamline segments defined by the geometry locations marked $\times$. The local flow is in the direction of the unit vector s, which for consistency must be related to the streamline grid as indicated in Fig. 1. $\boldsymbol{A}$ and $\boldsymbol{B}$ are the normal area vectors of the cell faces, with $\boldsymbol{B}$ representing the vector sum of the contributions from the two parts of the bent streamline cell faces. As shown in Fig. 2, the density ρ, speed q, and pressure p are located at the midpoints of the pseudonormal cell faces, with the total velocity vector simply $\boldsymbol{q} = q\boldsymbol{s}$. Because the streamline cell faces are defined to have no convection across them, only the pressure (denoted differently by Π for clarity) needs to be defined there.

The mass equation reduces to a statement that the flux along the streamtube is constant.

$$m = \rho_1 \boldsymbol{q}_1 \cdot \boldsymbol{A}_1 = \rho_2 \boldsymbol{q}_2 \cdot \boldsymbol{A}_2 \tag{4}$$

Similarly, the energy equation reduces to a statement that the total enthalpy does not vary along a streamtube.

$$h_0 = \frac{\gamma}{\gamma-1}\frac{p_1}{\rho_1} + 1/2\; q_1^2 = \frac{\gamma}{\gamma-1}\frac{p_2}{\rho_2} + 1/2\; q_2^2 \tag{5}$$

Because there is no mass flux across the streamline faces, the momentum equation reduces to

$$p_1\boldsymbol{A}_1 + m\boldsymbol{q}_1 + \Pi^-\boldsymbol{B}^- = p_2\boldsymbol{A}_2 + m\boldsymbol{q}_2 + \Pi^+\boldsymbol{B}^+ \tag{6}$$

In Ref. 6, it is shown that, to obtain a closed set of equations, the following consistency relation is required:

$$p_1 + p_2 = \Pi^+ + \Pi^- \tag{7}$$

To capture shocks in transonic solutions, the velocity in the momentum equation is replaced by an upwinded average. A numerical analysis in Ref. 7 proves that this is necessary to obtain a well-posed problem and provides a value for the optimum amount of upwinding in order to achieve sharp shocks. It is also shown that this upwinding is equivalent to a numerical bulk viscosity.

III. Boundary Conditions

Airfoil Surface

At the streamline that defines the surface of the airfoil, one boundary condition is required. In the analysis mode, this condition is the prescribed position of the streamline and, hence, the geometry of the airfoil. When the airfoil has a blunt leading edge, as is usually the case, the stagnation point at which the stagnation streamline joins the airfoil surface is allowed to "float" along the airfoil surface to ensure that there is no pressure jump across the stagnation streamline.

In the mixed inverse design mode, a desired pressure distribution is specified along most of the suction surface of the airfoil, and the geometry is specified for the remainder of the airfoil, as shown in Fig. 3. At the blend points between the inverse section and the rest of the airfoil, one specifies both the pressure and the geometry. Because this is now overspecified, one must introduce two degrees of freedom P_0 and P_1 into the target pressure distribution.

$$\Pi(\sigma) = \Pi_{\text{spec}}(\sigma) + P_0(\sigma-\sigma_0) + P_1(\sigma-\sigma_1) \tag{8}$$

In this equation, σ is the fractional arc length along the surface, and σ_0 and σ_1 correspond to the two blend points. The two degrees of freedom are then determined by the two constraints that there is no movement of the blend points. In this manner, geometric continuity of the airfoil surface is enforced. Additional degrees of freedom can be introduced to ensure that the surface slope is also continuous at the blend points.

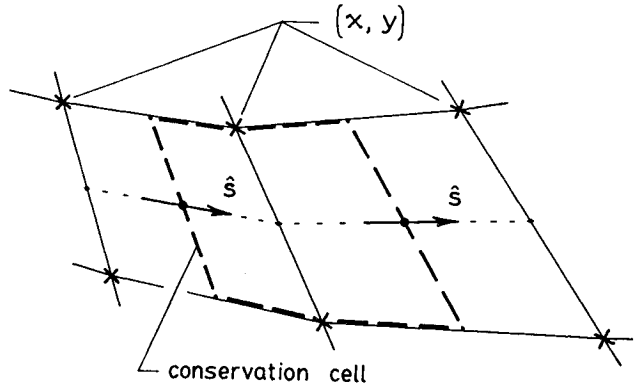

Fig. 1 Geometry node locations and conservation cell and s unit vector definitions.

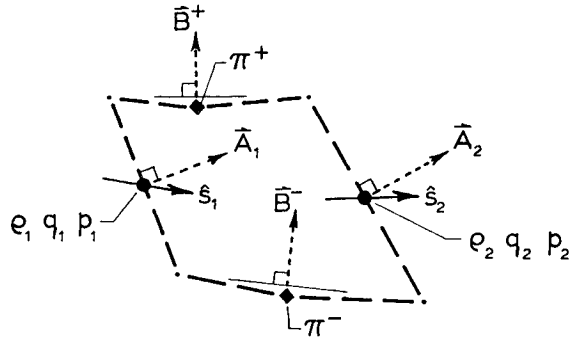

Fig. 2 State variable and area vector locations.

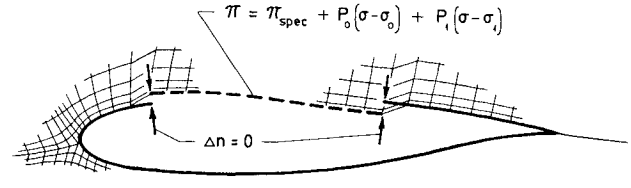

Fig. 3 Geometry continuity constraints for inverse problem.

The boundary conditions on the airfoil surface can also be modified to include viscous effects by specifying that the surface streamline is displaced from the surface of the airfoil by a distance equal to the displacement thickness of the boundary layer. The displacement thickness and other boundary-layer variables are calculated using a coupled integral boundary-layer analysis. Full details of the analytic integral boundary-layer equations, a transition model, and the numerical implementation of these are presented in another paper,[12] which demonstrates the method's ability to predict transition, separation bubbles, and overall drag.

Stagnation Streamline

The stagnation streamline both upstream and downstream of the airfoil is treated like any other streamline, by requiring that the pressure is continuous across it. When boundary-layer coupling is included, the two stagnation streamlines in the wake are separated by the wake displacement thickness.

Far Field

In addition to specifying the mass and total enthalpy in each streamtube, one boundary condition is required at the inflow and outflow planes and on the two outermost streamlines. One of the features of the ISES program is its ability to treat three different far-field treatments, corresponding to a wind-tunnel experiment (with solid wall), a freejet experiment (in which the outer two streamlines are constant pressure surfaces), and the normal case of an isolated airfoil.

Solid-Wall Wind Tunnel

In the case of a solid wall calculation, the far-field treatment is very simple. The position of the outer two streamlines and the flow angle at the inlet and outlet planes are fixed. In order to satisfy the Kutta condition at the trailing edge of the airfoil, the relative mass flux above and below the airfoil is allowed to vary.

Freejet

For freejet calculations, the pressure on the outer streamlines is specified, and the average of the inflow and outflow angles is fixed. The difference between the inflow and outflow angles is allowed to vary in order to satisfy the Kutta condition.

Isolated Airfoil

This is the most complex of the three far-field treatments. Because the Newton solution method, to be described in the next section, becomes expensive when many streamtubes are used, we aim to minimize the distance to the computational far-field boundary by using a second-order approximation to the far-field behavior of the flow around an isolated airfoil. Assuming for simplicity that the coordinate system is aligned with the freestream flow, the far-field potential is given by

$$\Phi = x + \frac{\Sigma}{2\pi}\log(r) - \frac{\Gamma}{2\pi}\theta + \frac{D_x}{2\pi}\frac{\cos(\theta)}{r} + \frac{D_y}{2\pi}\frac{\sin(\theta)}{r} + \left(\frac{\Gamma M_\infty}{2\pi}\right)^2\left(E\frac{\log(r)}{r}\cos(\theta) + F\frac{\cos(3\theta)}{r}\right) \tag{9}$$

where

$$\beta^2 = 1 - M_\infty^2 \tag{10}$$

$$\theta = \tan^{-1}(\beta y/x) \tag{11}$$

$$r^2 = (x/\beta)^2 + y^2 \tag{12}$$

$$E = \frac{1}{4}\left(\frac{\gamma+1}{\beta^3} + \frac{3-\gamma}{\beta}\right) \tag{13}$$

$$F = \frac{-1}{16}\left(\frac{\gamma+1}{\beta^3} + \frac{\gamma+1}{\beta}\right) \tag{14}$$

The derivation of this approximation from the nonlinear small-perturbation potential equation is given in Ref. 7 and is consistent with an earlier derivation by Ludford.[13] Σ is an equivalent source term due to entropy generation by shocks (and the displacement thickness of the wake when boundary-layer coupling is included) and is set explicitly in the program. Γ is the circulation that is allowed to float in order to satisfy the Kutta condition. D_x and D_y are the unknown doublet strengths, and the Γ^2 term is the leading-order nonlinear term in the far-field expansion. Terms proportional to Σ^2 and $\Sigma\Gamma$ have been neglected.

The boundary conditions which are used specify the inflow and outflow angles and the outer streamline pressures based

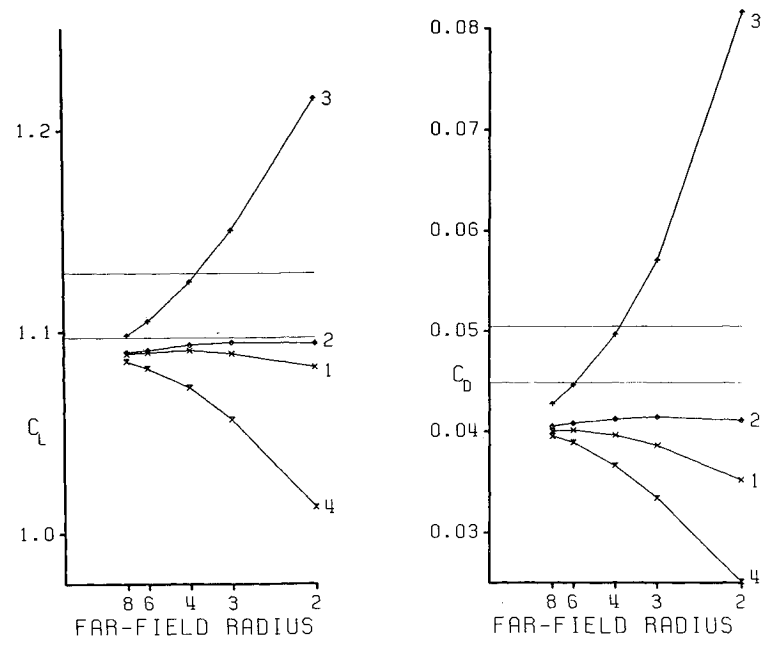

Fig. 4 Lift and drag coefficients for RAE 2822, $\alpha = 3.0$ deg, $M_\infty = 0.75$; 1) vortex only, 2) vortex and doublets, 3) solid wall, 4) freejet.

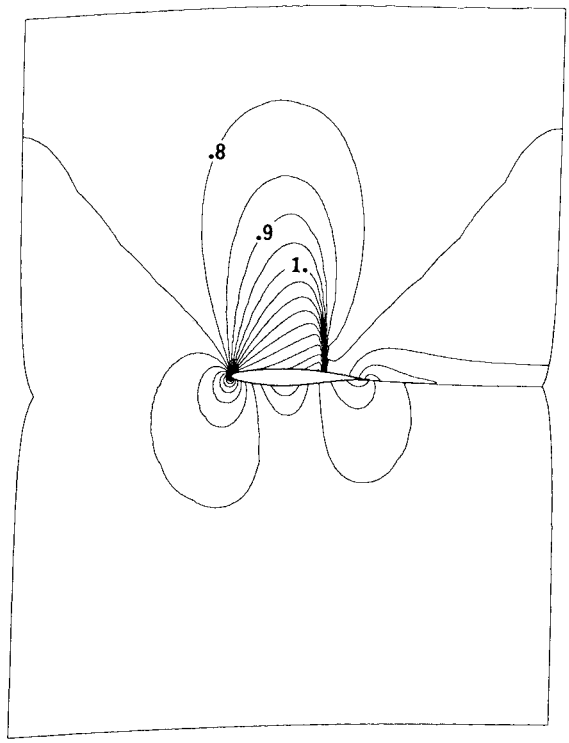

Fig. 5 Mach number contours for RAE 2822, using vortex and doublet far field; contour interval 0.05.

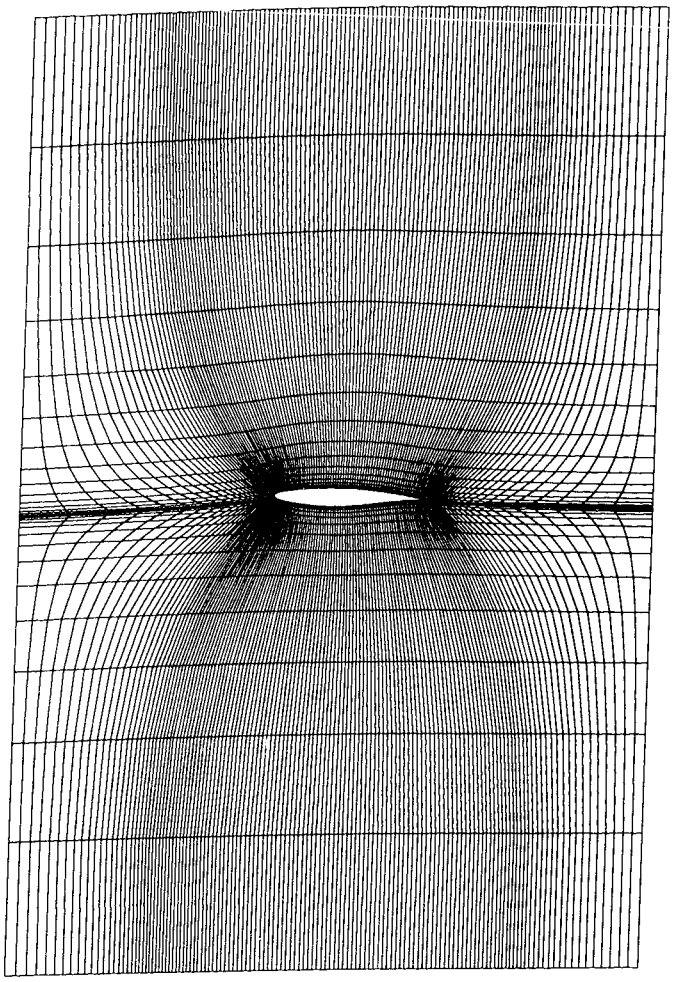

Fig. 6 Final streamline grid for RAE 2822 calculation.

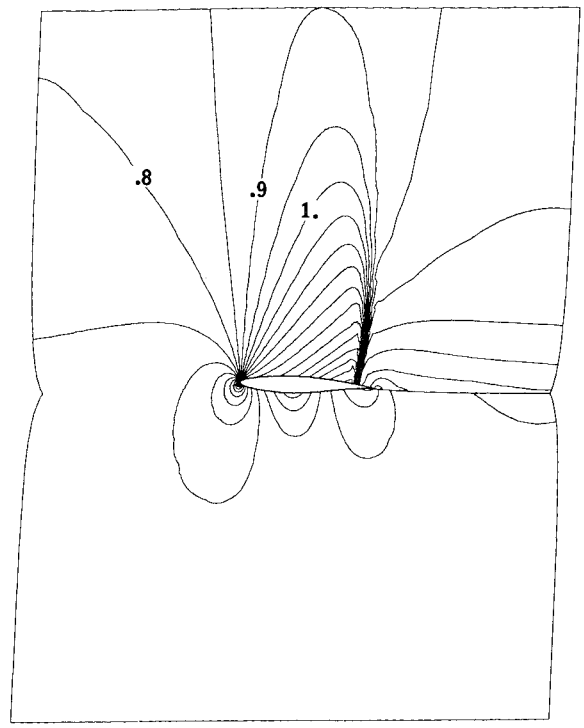

Fig. 7 Mach number contours for RAE 2822, using solid-wall far field; contour interval 0.05.

on this far-field expansion. The doublet strengths are determined iteratively by minimizing the inconsistency between the tangent to the outer streamlines and the flow direction obtained from $\nabla\Phi$. Further details are available in Ref. 7.

IV. Newton Solution Procedure

Conceptually, the Newton solution procedure is extremely simple. The system of nonlinear equations to be solved can be written as

$$F(Q) = 0 \tag{15}$$

where Q is the vector of flow variables and geometry variables and F is the vector of equations. At some iteration level ν, the Newton solution procedure is

$$F^\nu + \left[\frac{\partial F}{\partial Q}\right]^\nu \delta Q^\nu = 0 \tag{16}$$

$$Q^{\nu+1} = Q^\nu + \delta Q^\nu \tag{17}$$

In Refs. 6 and 7, it is shown that the solution of Eq. (16) to obtain δQ^ν requires the solution of a block-tridiagonal equation in which the blocks have dimension $2J$, (where J = number of streamlines) and there are I blocks along the principal diagonal (where I = number of streamwise stations along each streamtube). Thus, the computational work is proportional to IJ^3, which limits the number of streamtubes one can use and remain efficient. All the calculations in this paper were performed on grids with $I = 132$, $J = 32$. These took approximately 3 min per Newton iteration on a Micro Vax II. The advantage of the Newton methods is that very few iterations are required to obtain convergence. In theory, the convergence is quadratic and, in practice, the number of iterations required ranges from only 3 for a subsonic, inviscid case, up to 15 for a transonic case with a strong shock and boundary-layer coupling.

V. Study of Far-Field Effects

In this section, we examine the effect of the three different far-field treatments and evaluate the effectiveness of the

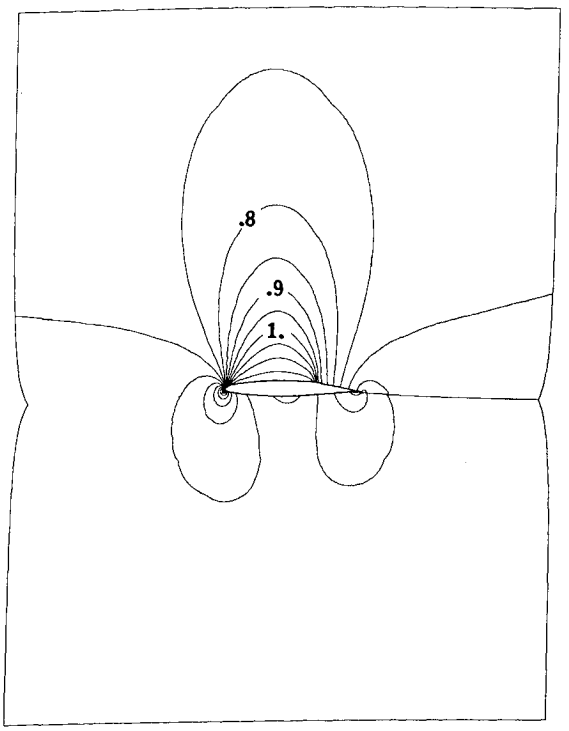

Fig. 8 Mach number contours for RAE 2822, using freejet far field; contour interval 0.05.

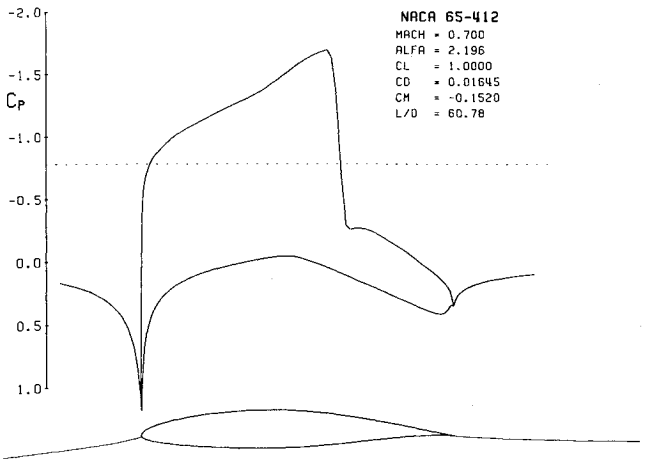

Fig. 9 Pressure distribution for NACA 65-412.

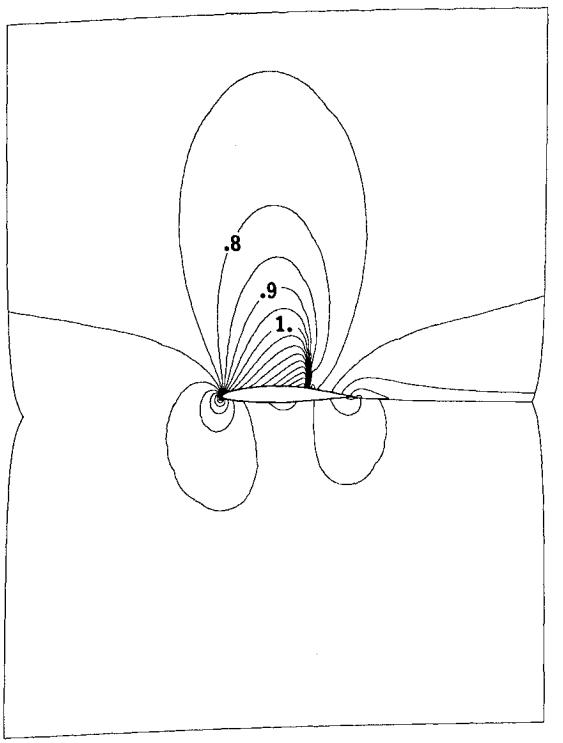

Fig. 10 Mach contours for NACA 65-412; interval 0.05.

higher-order doublet correction for the isolated airfoil in allowing the far-field boundary to be brought closer to the airfoil. The test problem is AGARD 06, the sixth of a set of test cases proposed by the AGARD Working Group 07,[14] which has been calculated by a number of researchers. AGARD 06 is an RAE 2822 airfoil at an angle of attack of 3.0 deg and a freestream Mach number of 0.75.

In the current results, four different far-field boundary conditions are used: 1) isolated airfoil boundary conditions, neglecting the doublet corrections; 2) isolated airfoil boundary conditions, including the doublet corrections; 3) solid-wall boundary conditions; and 4) freejet boundary conditions. The inflow and outflow boundaries were placed r_∞ chords upstream and downstream of the airfoil's center of lift, and the outer two streamlines were placed approximately r_∞/β chords above and below the airfoil, in accordance with the Prandtl-Glauert transformation. For each of the four far-field boundary treatments, five cases were run with $I=132$, $J=32$, so that increasing the far-field radius was at the expense of decreased resolution near the airfoil.

Figure 4 shows the predicted lift coefficients, together with a band corresponding to the numerical results published in the report of the AGARD Working Group.[14] Figure 4 also shows the corresponding predicted drag coefficients.

The calculations of the isolated airfoil with and without the doublet corrections clearly demonstrate the magnitude of the doublets' effect. Without the doublet corrections, the lift and drag vary by 1 and 12%, respectively, as r_∞ is reduced to 2 while, with the doublet corrections, the variations are only 0.3 and 1.5%. These remaining variations in lift and drag are probably due primarily to the varying grid resolution in the immediate vicinity of the airfoil.

Figure 5 shows the Mach number contours for the calculation with doublet corrections and $r_\infty=2$. Note that the sonic line extends almost halfway toward the upper outer streamline. If the far-field boundary were brought in any closer, then the assumption of small perturbations, upon which the small-perturbation nonlinear potential equation and the second-order expansion are based, would clearly become invalid. As it is, the maximum Mach number perturbation on the outer streamline is approximately 0.06. Figure 6 shows the final streamline grid.

The lift predictions are in reasonable agreement with the AGARD results.[14] Greater grid resolution in the neighborhood of the shock would be necessary to improve the results. The drag predictions are 10% lower than the AGARD results. We do not currently know why this is, but very similar results ($C_l=10.85$, $C_d=0.041$) have also been obtained by Dannenhoffer and Baron[15] using an adaptive grid method.

The calculations with the solid-wall and freejet boundary conditions indicate the magnitude of the corrections required for each type of experiment. In the solid-wall case, the variation in lift and drag are 11 and 90%, respectively, while, in the freejet case, they are 7.5 and 35%. Clearly, for an experiment of the same dimension, the freejet approach gives much better predictions than wind tunnels with solid walls. These results also show that the current numerical method can be used to assess experimental errors and evaluate the corrections necessary to interpret experimental data.

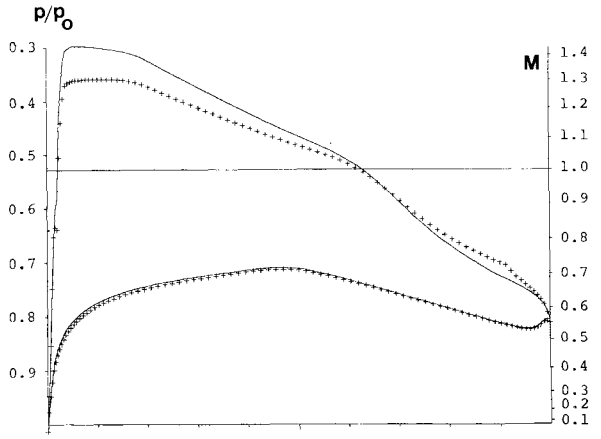

Fig. 11 Specified (line) and resultant (symbols) pressure distribution for design 1.

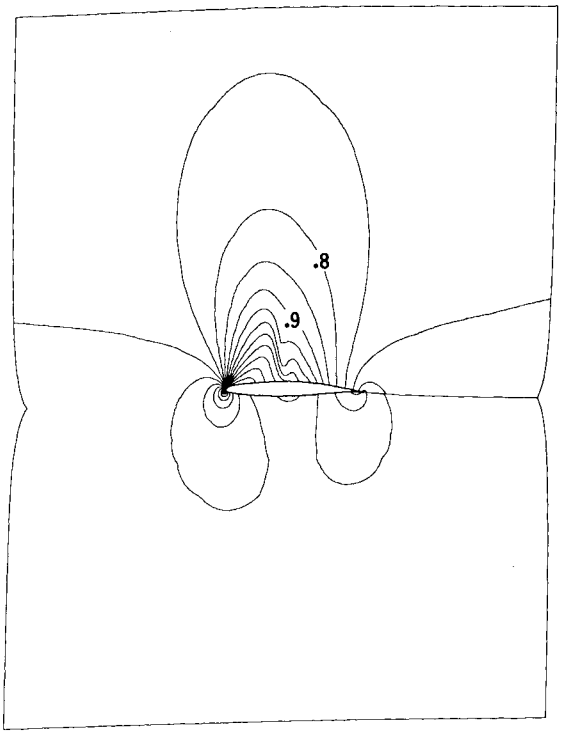

Fig. 12 Mach contours for design 1; interval 0.05.

Figures 7 and 8 show the Mach number contours corresponding to the solid-wall and freejet calculations for $r_\infty = 2$. In the solid wall case, note that the shock has strengthened and moved rearward while, in the freejet case, the shock has weakened and moved forward. The constant pressure surface at the outer streamlines is obvious in the freejet case due to the absence of any contours reaching the outer streamlines.

VI. Example of Transonic Design

In this section, we present an example of using ISES to design a transonic airfoil. The objective was to design a transonic airfoil with a lift coefficient of 1.000 at a freestream Mach number of 0.7 and Reynolds number of 10^7. In addition, we wished it to have an acceptable off-design performance.

The starting point for the design procedure was a known airfoil, the NACA 65-412. One option in ISES is to allow the angle of attack to vary in order to achieve a specified lift

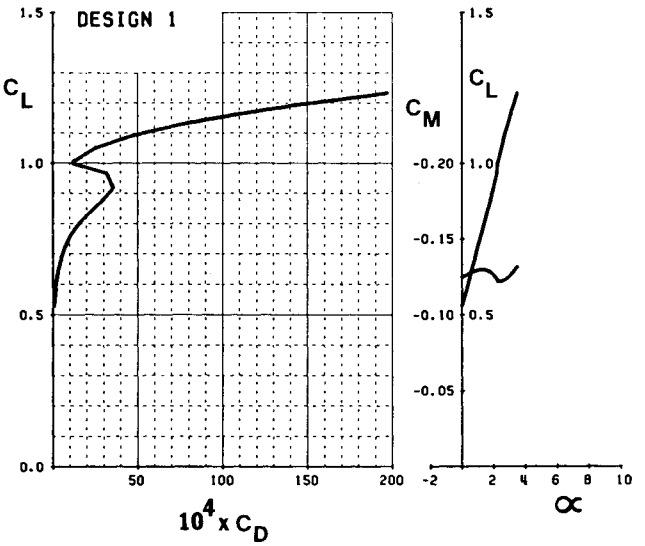

Fig. 13 Lift-drag polar for design 1.

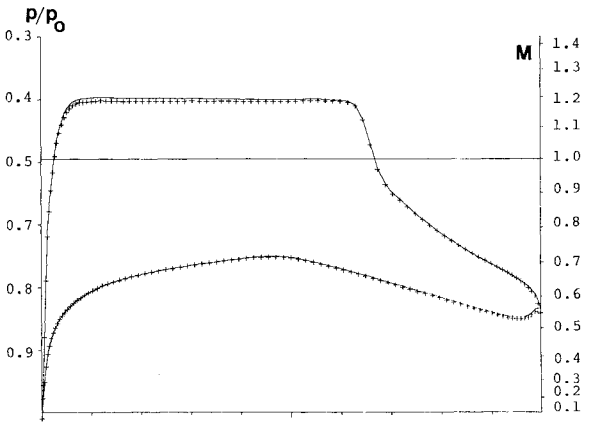

Fig. 14 Specified (line) and resultant (symbols) pressure distributions for design 2.

coefficient. Using this option, with $C_l = 1.000$ and $M_\infty = 0.7$, ISES gave the solution shown in Figs. 9 and 10. A strong shock has formed on the suction surface, leading to a high wave drag.

The first attempt to design an improved airfoil allowed the geometry to vary along almost the entire length of the suction surface and specified a shock-free surface pressure distribution with its minimum near the leading edge. Figure 11 shows the specified pressure distribution and the pressure distribution corresponding to the solution produced by ISES. The difference is due to the two degrees of freedom that were introduced to satisfy geometric continuity. Figure 12 shows the Mach contours, revealing that there is a very weak displaced shock just off the airfoil surface. For this reason, the drag coefficient $C_d = 0.0012$.

To examine the airfoil's off-design performance, the program was switched into analysis mode, and a lift-drag polar was calculated by varying the angle of attack α while keeping the freestream Mach number fixed. The polar calculation is an automated procedure which, in this case, incremented α in steps of 0.2 deg and reconverged the solution each time in only one or two Newton iterations. This feature makes ISES very efficient for analyzing a range of off-design performance. Figure 13 shows that the drag increases noticeably, not only at higher α but also at slightly lower α.

An alternative design was produced by specifying a suction surface pressure distribution with a "flat rooftop" profile terminated by a rapid diffusion. Figure 14 shows the

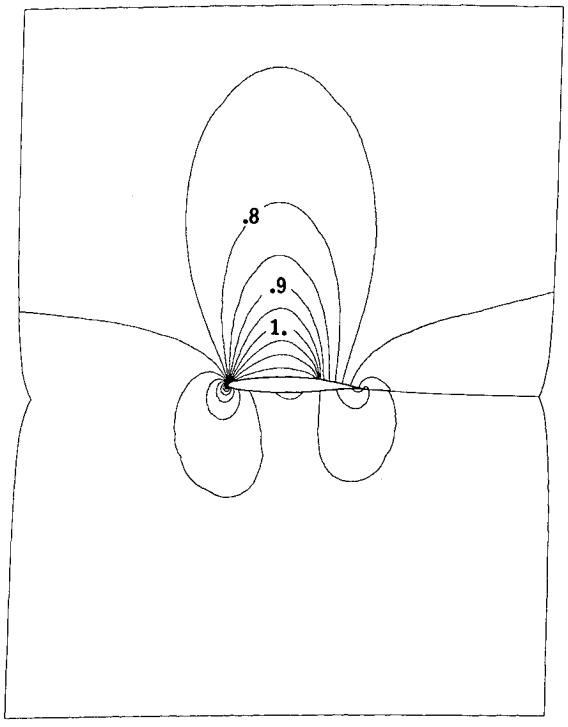

Fig. 15 Mach contours for design 2; interval 0.05.

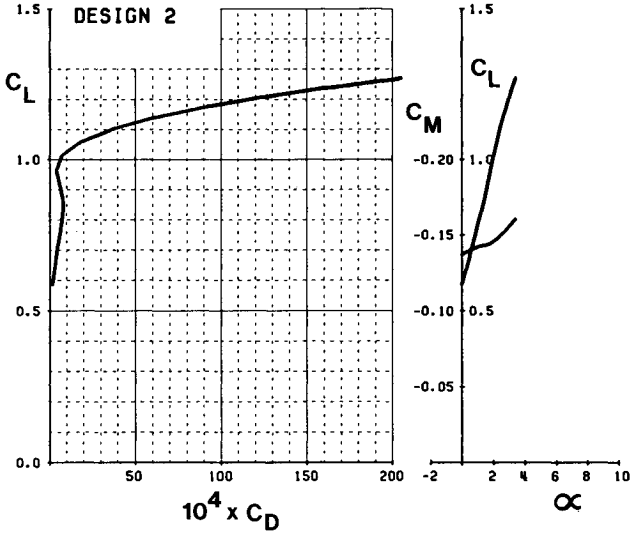

Fig. 16 Lift-drag polar for design 2.

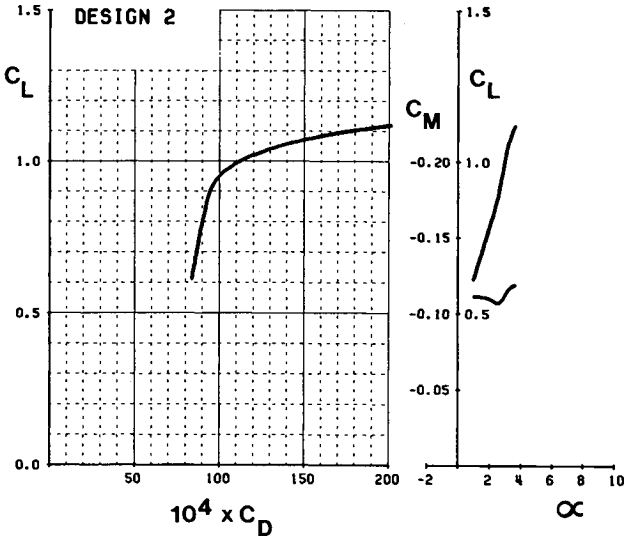

Fig. 17 Lift-drag polar for design 2, including boundary-layer coupling ($Re = 10^7$).

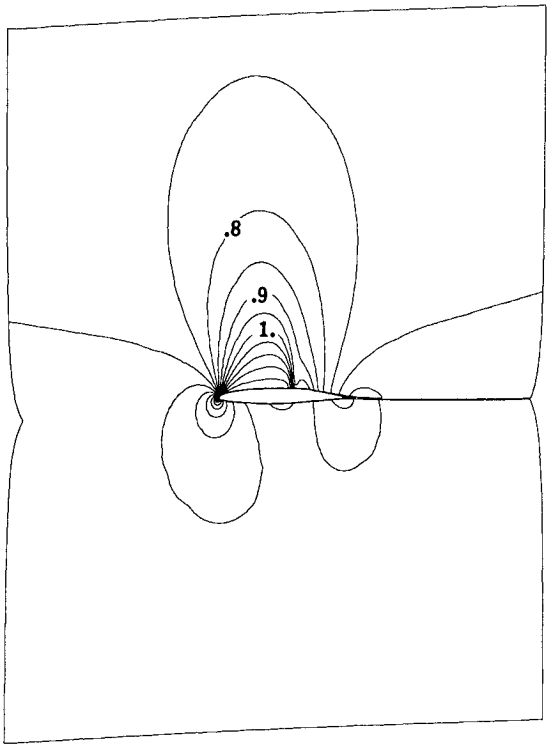

Fig. 18 Mach contours for design 2, including boundary-layer coupling; interval 0.05.

specified and resultant pressure distributions. Figure 15 shows the Mach contours. In this case, there is no displaced shock, and $C_d = 0.0006$, owing to the very rapid pressure diffusion on the surface, which numerically is equivalent to a very weak shock. Figure 16 shows the corresponding lift-drag polar. The off-design performance is now much better, particularly at lower angles of attack.

Having decided that the second design was the better of the two, we next included the boundary-layer coupling in order to examine the importance of viscous effects. The Reynolds number was specified to be 10^7, and the transition points on both surfaces were specified at 15% chord. Figure 17 shows the lift-drag polar, and Fig. 18 shows the Mach contour plot at the design point of $C_l = 1.000$. The angle of attack at the design point has increased to $\alpha = 2.95$ deg from the inviscid value of $\alpha = 1.95$ deg. The Mach number in the "rooftop" section has increased, and the shock has strengthened and moved forward slightly. The total drag has obviously increased owing to the viscous drag, but the wave drag component (which is calculated from the entropy generation in the shock) has increased only slightly and, at the design point, represents only 17% of the total drag. The rapid increase in total drag at higher C_l is due to a rapid increase in wave drag.

Figure 19 compares the original NACA 65-412 airfoil with the final design airfoil. For clarity, the y direction has been magnified five times in the figure. It can be seen that the designed airfoil is smoothly continuous, with no indication

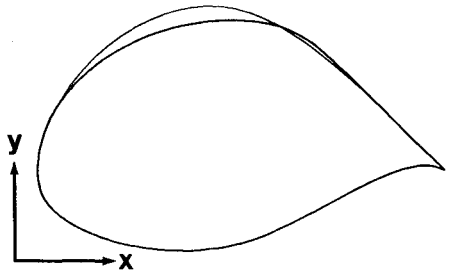

Fig. 19 Comparison of original NACA 65-412 airfoil (thin line) and new design 2 airfoil (thick line); the y direction is magnified 5 times.

of the location of the blend points. Overall, this design is a satisfactory solution to the design problem that was posed.

In some cases, it is possible to include the viscous coupling in the design mode. There can be some major difficulties, however. The problem is that the design mode, in which the pressure is specified, corresponds to what is referred to as the "direct" mode for boundary-layer calculations (an unfortunate clash of definitions), in which dU_e/dx is specified. It is well known that this is not a well-posed problem when the boundary layer separates,[16] and so the inverse design mode, including boundary-layer coupling, will fail if, by chance, the boundary layer separates. Therefore, it is generally more robust to follow the procedure used here, with an inviscid design followed by a viscous analysis.

VII. Conclusions

This paper has demonstrated the capabilities of a new two-dimensional transonic design method based on the solution of the Euler equations on an intrinsic streamline grid, with the option of specifying either direct or inverse boundary conditions at the airfoil surface.

The use of a second-order approximation to the far-field flow improves the accuracy and allows the far-field boundary to be brought much closer to the airfoil surface. In addition, numerical results show the sensitivity of experiments, with both solid-wall wind tunnels and freejets, to the placement of the far-field boundary. Freejet results are shown to be significantly better than results obtained with solid-wall wind tunnels. The numerical method could also be used to calculate experimental corrections for both of these types of experiments.

The design capabilities of the new method were demonstrated by designing a transonic airfoil with $C_l = 1.000$ at $M_\infty = 0.70$. A comparison of two designs shows that the off-design performance is improved by specifying a surface pressure distribution with a very weak shock. The final lift-drag polar, which includes viscous effects through a coupled boundary-layer analysis, shows that the designed airfoil is a satisfactory solution to the design task.

Acknowledgments

This research was supported by Air Force Office of Scientific Research Contract F49620-78-C-0084, supervised by Dr. James D. Wilson.

References

[1]Vanderplaats, G. N., "An Efficient Algorithm for Numerical Airfoil Optimization," AIAA Paper 79-0079, Jan. 1979.

[2]Hicks, R. M., "Transonic Wing Design Using Potential Flow Codes—Successes and Failures," SAE Paper 810565, 1981.

[3]Lighthill, M. J., "A New Method of Two-Dimensional Aerodynamic Design," Aeronautical Research Council, R&M 2112, June 1945.

[4]Volpe, G. and Melnik, R. E., "The Design of Transonic Airfoils by a Well-Posed Inverse Method," Presented at the International Conference on Inverse Design Concepts in Engineering Sciences, Austin, TX, Oct. 1984.

[5]Bauer, F., Garabedian, P., Korn, D., and Jameson, A., "Supercritical Wing Sections I, II, III," *Lecture Notes in Economics and Mathematical Systems*, Springer-Verlag, New York, 1972, 1975, 1977.

[6]Giles, M. B., "Newton Solution of Steady Two-Dimensional Transonic Flow," Massachusetts Institute of Technology, Cambridge, MA, Gas Turbine Laboratory Rept. 186, Oct. 1985.

[7]Drela, M., "Two-Dimensional Transonic Aerodynamic Design and Analysis Using the Euler Equations," Massachusetts Institute of Technology, Cambridge, MA, Gas Turbine Laboratory Rept. 187, Feb. 1986.

[8]Drela, M., Giles, M. B., and Thompkins, W. T., "Newton Solution of Coupled Euler and Boundary Layer Equations," *Third Symposium on Numerical and Physical Aspects of Aerodynamic Flows*, California State Univ., Long Beach, CA, Jan. 1985, pp. 2-1—2-8.

[9]Giles, M. B., Drela, M., and Thompkins, T., "Newton Solution of Direct and Inverse Transonic Euler Equations," AIAA Paper 85-1530, July 1985.

[10]Giles, M. B., "Solution of One-Dimensional Euler Equations Using a Box Method," Massachusetts Institute of Technology, Cambridge, MA, CFDL Tech. Rept. 84-1, Feb. 1984.

[11]Wornom, S., "Application of Two-point Difference Schemes to the Conservative Euler Equations for One-Dimensional Flows," NASA TM-83262, May 1982.

[12]Drela, M. and Giles, M. B., "Viscous-Inviscid Analysis of Transonic and Low Reynolds Number Airfoils," *AIAA Journal*, to be published.

[13]Ludford, G. S. S., "The Behavior at Infinity of the Potential Function of a Two-Dimensional Subsonic Compressible Flow," *Journal of Mathematical Physics*, Vol. 30, 1951, pp. 117–130.

[14]AGARD Working Group 7, "Test Cases for Inviscid Flow Field Methods," AGARD Rept. AR-211, 1985.

[15]Dannenhoffer, J. F. and Baron, J. R., "Robust Grid Adaptation for Complex Transonic Flows," AIAA Paper 86-0495, Jan. 1986.

[16]Brown, S. N. and Stewartson, K., "Laminar Separation," *Annual Review of Fluid Mechanics*, Vol. 1, 1969, p. 45.